# Variations of surface roughness on inhomogeneous underlying surface at Nagqu Area over the Tibetan Plateau

Maoshan Li[*1], Lei Shu[1], Xiaoran Liu[1], Shucheng Yin[1], Lingzhi Wang[1], Wei Fu[1], Genhou Sun, Yaoming Ma [2], Fanglin Sun [3]

（1.School of Atmospheric Sciences/Plateau Atmosphere and Environment Key Laboratory of Sichuan Province/Joint Laboratory of Climate and Environment Change, Chengdu University of Information Technology, Chengdu 610225, Sichuan China;

2. Key Laboratory of Tibetan Environment Changes and Land Surface Processes, Institute of Tibetan Plateau Research, Chinese Academy of Sciences, CAS Center for Excellence in Tibetan Plateau Earth Sciences, Beijing, China;

3. Key Laboratory of Land Surface Process and Climate Change in Cold and Arid Regions, Chinese Academy of Sciences. Lanzhou, China）

**Abstract：** Using the MODIS satellite data and station atmospheric turbulence observation data in Nagqu area of northern Tibetan plateau in 2008, 2010 and 2012, with the Massman retrieved model and the measured values of average wind speed and turbulent flux of a single height ultrasonic anemometer to determine aerodynamic surface roughness, the temporal and spatial variation characteristics of the surface roughness was analyzed. The results show that the surface roughness length has obvious seasonal variation characteristics. From February to August, Z0m increases constantly with the ablation of snow and vegetation growth, and the maximum value reaches 4-5cm at BJ site. From September to February, Z0m gradually decreased because of the post-monsoon over the plateau, and the values decreased to about 1-2cm. The snowfall in abnormal years is the main reason why Z0m is obviously lower than that in normal. The underlying surface can be divided into four categories according to the different values of Z0m: snow and ice, sparse grassland, lush grassland and town. Among them, lush grassland and sparse

* Corresponding author

Dr. Maoshan Li

Chengdu University of Information Technology

24 Block 1, Xuefu Road, Chengdu 610225, Sichuan, China

E-mail: lims@cuit.edu.cn

grassland account for 62.49% and 33.74% respectively in the region, which are the main categories, and their Z0m annual changes are between 2-6cm and 1-4cm. The correlation between the two methods are positively related to each other, and the retrieved data are smaller than the measured results due to the average sliding action. On the whole, Z0m calculated by satellite data retrieved algorithm is feasible, it can be applied to improve the model parameters of land surface model parameters and the accuracy of model simulation, better reveal the heat flux exchange.

**Key words:** Northern Tibet Plateau；Surface roughness；NDVI；MODIS

# 1 Introduction

Known as the "third pole" of the earth (Jane, 2008), the Tibetan plateau has an average altitude of over 4000m, accounting for a quarter of China's territory. It is located in the southwest of China, adjacent to the subtropical tropics in the south and reaching the mid-latitude in the north, making it the highest plateau in the world. Due to its special geographical location and geomorphic characteristics, it plays an important role in the formation, outbreak, duration and intensity of Asian monsoon especially in the global climate system. (Yang et al., 1998; Zhang et al., 1998; Wu et al., 1999, 2004, 2005; Ye et al, 1998; Wu et al, 1998; Tao et al, 1998). Lots of research shows that (Wu et al., 2013; Wang, 1999; Ma et al, 2002) the land-atmosphere interaction on the Tibet plateau plays an important role in regional and global climate. Wang (Wang, 1999) pointed out that high latitude areas and mountainous areas are sensitive areas of climate change, especially the land-atmosphere interaction located in the plateau area of middle latitude (including large areas of permafrost), which plays an extremely important role in regional climate and global climate. The plateau monsoon is closely related to the intensity and location of the south Asian high (Xun et al, 2002). The correlation between the dynamic index of plateau monsoon and the pelagic meridional wind shows that there is a teleconnection in summer, indicating that the teleconnection is the relationship between the plateau monsoon, the East Asian monsoon and the South Asian monsoon. In the past 47 years, the Tibetan plateau has shown a significant warming trend and increased precipitation. (Li et al., 2010) The thermal effects of the Tibetan Plateau not only have an important impact on the Asian monsoon and precipitation variability, but also affect

the atmospheric circulation and climate in North America and Europe and the South Indian Ocean by inspiring large-scale teleconnections similar to the Asia-Pacific Oscillation. (Zhou et al., 2009).

The various thermal and dynamic effects of the Tibetan Plateau on the atmosphere affect the free atmosphere through the atmospheric boundary layer. Therefore, it is particularly important to analyze the micro-meteorological characteristics of the atmospheric boundary layer of the Qinghai-Tibet Plateau, especially the near-surface layer. (Li et al., 2000). Affected by the unique underlying surface conditions of the Tibetan Plateau, local heating shows interannual and interdecadal variability (Zhou et al., 2009). Land-atmosphere interaction refers to a series of complex processes such as thermodynamics, dynamic, hydrology, biophysical and biochemical processes that occur on land surface, and the interaction process between these processes and the atmosphere (Su et al., 1999). Different underlying surfaces have different diversity, complex composition and uneven distribution. They also make the land surface composed of them diverse and complex. As the main input of atmospheric energy, the surface greatly affects the various interactions between the ground and the atmosphere, and even plays a key role in local areas or specific time (Guan et al, 2009). For this reason, the study of the land-atmosphere interaction on the Tibetan Plateau has become one of the research hotspots in the past 30 years, and has received more and more attention on the whole world.

The climate system is sensitive to anomalous changes in land surface conditions. The surface characteristic parameters (dynamic roughness, thermodynamic roughness, etc.) play an important role in the land surface process and are important factors in causing climate change (Jia et al., 2000). There are different degrees of fluctuant on the underlying surface of the Tibetan Plateau, which brings certain obstacles to understanding the land-atmosphere interaction of the Tibetan Plateau. The fluctuant surface may alter the arrangement of roughness element which on the surface and cause changes in surface roughness. Changes in roughness can also affect changes in the characteristics of other surface turbulent transportation, which may also result in changes in surface fluxes. Chen et al., (2015) presents a practical approach for determining the aerodynamic roughness length at fine temporal and spatial resolution over the landscape by combining remote sensing and ground measurements. And the surface roughness is an important parameter in the

land surface model and climate model. Its size reflects the matter energy exchange, transmission intensity and interaction between the near surface airflow and the underlying surface to some extent. (Liu et al., 2007; Irannejad et al, 1998; Shao et al, 2000; Zhang et al., 2003). Zhou et al. (2012) demonstrated that simulated sensible heat flux compared with measurement was significantly improved by using a time-dependent z0m. Therefore, the primary objective of this study is to calculate the surface roughness and its variation characteristics so that furthermore understanding of land-atmosphere interactions on the central of the Tibetan Plateau.

The Nagqu area is located in the hinterland of the Tibetan Plateau, in the north of Tibet. It is the source of the Yangtze River, the Nujiang River, the Lhasa River and the Yigong River. The entire terrain is high in the west and low in the east, with an average elevation of more than 4,500 meters. The altitude is high, the heat is insufficient, the climate is severely cold and dry, and the oxygen content is only half of the sea level. The northern Tibet Plateau is one of the most severe areas in Tibet. It is a typical sub-frigid climate zone. It is cold and lack of oxygen, the climate is dry, the temperature difference between day and night is large, and it is windy. (Li et al., 2004) However, there is a vast natural grassland here, so a complete mesoscale observation network centered on the Nagqu climate observation and research station has been established, and a large amount of valuable observation data has been obtained for more accurate description to provide sufficient evidence for Plateau land-atmosphere interactions and atmospheric boundary layer structures. The underlying surface of the Nagqu area is a vast highland plain, and the vegetation is alpine grassland. However, the underlying surface has different degrees of ups and downs and has certain complexity, which brings certain difficulties for the meticulous profound study of the land-atmosphere interaction on the Tibetan Plateau.

In this study, the satellite data is obtained by MODIS, and the normalized difference vegetation Index (NDVI) in Nagqu area is used to study the dynamic surface roughness length. And using three observation stations in the region, atmospheric turbulence observation data from 2008, 2010, and 2012 and observation data from automatic weather stations, the measured values of average wind speed and turbulent flux of a single height ultrasonic anemometer for determining surface dynamics roughness Z0m is applied (Chen et al., 1993). Analyzed time-scale dynamics of

Z0m and the different results of different underlying surfaces. Through the comparison of the calculation results of the observation data, we study whether the surface roughness values retrieved by satellites are reliable, in order to provide accurate surface characteristic parameters for the study of land-atmosphere interaction in the plateau area, and improve the theoretical research level of the near-surface layer in the Tibetan Plateau. In the following section, we describe the case study area, the MODIS remote sensing data, the ground observations, and the land cover map used to drive the revised Massman model (Massman et al, 1997, 1999). In Section 3, we present the results, followed by a validation based on flux measurements on Nagqu station. Finally, we give some concluding remarks on variation characteristics of the aerodynamic roughness lengths on the Nagqu area in the central of the Tibetan Plateau.

# 2 Study area, Data and methods

## 2.1 Study area and Data

The area selected in this study is a 200×200km$^2$ area centered on the Nagqu Station of Plateau Climate and Environment of the Northwest Institute of Ecology and Environmental Resources, Chinese Academy of Sciences, Northern Tibet Plateau.

In this area, there are North Pam (Portable Automated Meso-net) Automatic Meteorological Observatory (NPAM), Nam Co Station for Multisphere Observation and Research, Chinese Academy of Sciences (NAMC), and BJ three meteorological observatories stations (Figure 1).The underlying surface around the observation point is relatively flat on a small spatial scale, and there is a certain undulation at a large spatial scale. The data used included observations from atmospheric turbulence and automatic meteorological stations.

The BJ station is located at 31.37°N, 91.90°E, and the altitude is 4509m a.s.l. The BJ observation point is located in the seasonal frozen soil area, and the vegetation is alpine grassland. The site measurement equipment includes ultrasonic anemometer (CAST3), CO2/H2O infrared open circuit analyzer (LI 7500) and automatic meteorological observation system. (Ma et al., 2006) This study uses the data from BJ station in 2008 and 2012. The NPAM station is located at 31°56’N, 91°43’E and has an altitude of approximately 4700m. The ground of the experimental

field is flat and the area is wide. The ground is covered by a plateau meadow 15 cm high in summer. The experimental station observation equipment includes ultrasonic wind thermometer and humidity probe pulsator, and also includes data on temperature and humidity, air pressure, average wind speed, average wind direction, surface radiation temperature, soil heat flux, soil moisture and temperature, and radiation. (Ma et al., 2006). The NAMC station is located at 30°46.44'N, 90°59.31'E, at an altitude of 4730m. It is located on the southeastern shore of Namco Lake in Namuqin Township, Dangxiong County, Tibet Autonomous Region. It is backed by the Nyainqentanglha Mountain Range and the underlying surface is an alpine meadow. This study uses the data from NPAM station for the whole year of 2012 and from NAMC station for the whole year of 2010.

**Figure 1 about here**

**Table 1 about here**

The land cover data used in this study is GLC2009 (Arino et al, 2010) data. The data is the retrieved data of Envisat satellite in 2009 with a spatial resolution of 300m and the classification standard is Land Cover Classification System (LCCS). The classification standard divides the global surface into 23 different types, and the selected area in this study includes 14 of them. As the actual situation in the selected area does not match the data part of GLC2009, there is no underlying surface such as farmland in the selected area. Therefore, according to the actual land cover types obtained by Chu (Chu, 2010), the names of irrigated farmland, dry farmland, mixed farmland vegetation, mixed multi-vegetation land, closed grassland and open grassland are replaced with 6 grassland, shrub meadows, mountain meadows, alpine grasslands, alpine meadows and sparse vegetation in the mountains. Since the proportion of the underlying surface of the tree as a whole is only 0.36%, the four types of underlying surfaces of the evergreen coniferous forest, the mixed forest, the multi-forest grassland mix and the multi-grass forest land mix will no longer be studied.

The satellite data from the MODerate-resolution Imaging Spectroradiometer (MODIS) is an important sensor in the satellites TERRA and AQUA launched by the US Earth Observing System Program. The band of MODIS sensor covers the full spectrum of visible light to thermal infrared,

which can detect surface and atmospheric conditions such as surface temperature, surface vegetation cover, atmospheric precipitation, cloud top temperature, etc. The maximum spatial resolution is 250m. The normalized vegetation index obtained by MODIS detection is the MYD13Q1 product from MODIS, which provides a global resolution of 250m per 16 days. This study selects 73 materials for the year of 2008, 2010 and 2012 in Nagqu.

## 2.2 Methodology

### 2.2.1 Method for calculating surface roughness by observation data

Using the measured values of average wind speed and turbulent flux of a single height ultrasonic anemometer, the calculation scheme of surface roughness proposed by Chen et al. (Chen et al., 1993) was selected and the dynamic variation of the surface roughness was obtained.

According to the Monin-Obukhov similarity theory (Monin et al., 1954), the wind profile formula with the stratification stability correction function (Panosky et al, 1984) is

$$U(z)=\frac{u_*}{k}\left[\ln\frac{z-d}{Z_{0m}}-\psi_m(\zeta)\right] \quad (1)$$

$$\psi_{\mathrm{m}}(\zeta)=2\ln(\frac{1+x}{2})+\ln(\frac{1+x^2}{2})-\tan^{-1}(x)+\frac{\pi}{2} \qquad \zeta<0 \quad (2)$$

$$\psi_m(\zeta)=-5\zeta \qquad \zeta>0 \quad (3)$$

Where: $u_*=\sqrt{-\overline{u'w'}}$ , Z0m is the dynamic surface roughness length; z is the observed height; d is zero plane displacement, taken as 0.03m, calculated from the average vegetation height 0.045m (Stanhill, 1969); U is the average wind speed; k is the Karman constant, taken as 0.40 (Högström,1996); $L=-\frac{u_*^3}{(k\frac{g}{\overline{\theta}})\overline{\theta'\omega'}}$ (Monin et al.， 1954 is the Monin-Obukhov length; $x=(1-16\zeta)^{1/4}$; $\zeta=(z-d)/L$ is the atmospheric stability parameter. Available from formula (2.1):

$$\ln\frac{z-d}{Z_{0m}}=\frac{kU}{u_*}+\psi_m(\zeta) \quad (4)$$

Using equations (2)~(4), Z0m can be determined by fitting $\zeta$ and observation of a single height $\frac{kU}{u_*}$.

**2.2.2 Method for calculating surface roughness by satellite data**

For fully covered uniform canopy，Brutsaert suggest that z 0m =0.13hv (Brutsaert, 1982). For the canopy with proportional coverage (partial coverage), according to the research of Raupach (Raupach, 1994), z 0m/hv varies with the leaf area index (LAI). However, Pierce et al. (Pierce et al. 1992) pointed out that for all kinds of biological groups, leaf area index can be obtained from NDVI, and the density grade of vegetation can be related to NDVI. Asrar et al (Asrar et al., 1992) pointed out that there was mutual relationship between LAI, NDVI and ground cover through the study of physical model. Moran's study (Moran, et al., 1994) gives another way, using a function of the relationship between NDVI and $Z_{0m}$ in the growing season of alfalfa,

$$Z_{0m}(x,y) = \exp\left[C_1 + C_2 NDVI(x,y)\right] \quad (5)$$

Where $C_1$ and $C_2$ are empirical constants.

Considering that the main underlying surface of the study area is grassland, this study selects the Massman model (Massman et al, 1997, 1999) to calculate the Z0m in Nagqu area of central of the Tibetan Plateau. The Massman model is calculated as follows:

$$\gamma = C_1 - C_2 \cdot exp(-C_3 \cdot C_d \cdot LAI) \quad (6)$$

$$n_{ec} = \frac{C_d \cdot LAI}{2 \cdot \gamma^2} \quad (7)$$

$$d_h = 1 - \frac{\left[1 - \exp(-2 \cdot n_{ec})\right]}{2 \cdot n_{ec}} \quad (8)$$

$$\frac{Z_{0m}}{h} = \left[1 - d_h\right] \cdot \exp\left(-\frac{k}{\gamma}\right) \quad (9)$$

Among them, $C_1$=0.32, $C_2$=0.26, $C_3$=15.1 is the constant in the model, which is related to the surface drag coefficient, LAI is the leaf area index, $C_d$=0.2 is the liquid surface drag coefficient, $n_{ec}$ is the wind speed profile coefficient of fluctuation in the vegetation canopy, h is the vegetation height. In many earlier studies, it was concluded that the high-altitude environment of the Tibetan Plateau caused a low temperature in the area to which the study was located, and had an effect on the height and sparseness of the vegetation. Based on the previous researches, this

study considers that the vegetation height in northern Tibet is related to the normalized differential vegetation index (NDVI) and altitude (Chen et al, 2013), and introduced the altitude correction factor on the original basis. The following is the calculation formula.

$$H = h_{\min} + (\frac{h_{\max} - h_{\min}}{NDVI_{\max} - NDVI_{\min}})(NDVI - NDVI_{\min}) \qquad (10)$$

$$h = acf \cdot H \qquad (11)$$

Among them, $h_{min}$ and $h_{max}$ are the minimum and maximum values of vegetation height observed at the observation station, and $NDVI_{max}$ and $NDVI_{min}$ are the maximum and minimum values of NDVI of the observation station. H is based on the assumption that the vegetation height is directly proportional to the NDVI. x is the altitude and is obtained from ASTER's DEM products. acf is the altitude correction factor (Chen et al., 2013), which is used to characterize the effect of altitude elevation on the height of vegetation in northern Tibet. Its form is:

$$acf = \begin{cases} 0.149, x > 4800 \\ 11.809 - 0.0024 \cdot x, 4300 < x < 4800 \\ 1.49, x < 4300 \end{cases} \qquad (12)$$

The LAI used in this thesis is calculated by the NDVI of MODIS (Su,1996). The calculation formula is:

$$LAI = \left( \frac{NDVI * (1 + NDVI)}{1 - NDVI} \right)^{0.5} \qquad (13)$$

# 3 Result analysis

## 3.1 The variation characteristics of surface roughness by using measured data

Figure 2 shows the temporal variation characteristics of surface roughness of sites in different years in Nagqu area. It can be seen that Z0m value has continued to increase since February to reach a maximum in July and August. The BJ station and the NPAM station in 2012 show that July is slightly larger than that in August, the 2010 NAMCO station and the 2008 BJ station in August is bigger than July. The BJ station may have a precipitation process in July 2008, resulting in a July Z0m value less than June. After August, Z0m began to decrease, and the value of December was about the same as the value of January. In general, the change of Z0m degree of

each station increases from spring to summer and decreases month by month from summer to winter.

**Figure 2 about here**

### 3.2 Spatiotemporal variation characteristics of surface roughness length retrieved by MODIS data

Figure 3 is a plot of surface roughness distribution of 200 × 200 $km^2$ around the BJ site in 2008. In February, the Z0m decreased from January, which may be due to snowfall, temperature, etc., resulting in a small Z0m and continued to decrease. Due to the rising temperature of snow melting, Z0m showed a slowly increasing trend from February to May, and Z0m showed a rapid increase from June to August. From June onwards, a large number of surface textures are presented, indicating the complexity of the underlying surface. Whether it is the bulk surface or the vegetation, which have an important impact on Z0m. From May to August, due to the obvious changes in humidity, temperature and pressure caused by the plateau summer monsoon, the height and coverage of surface vegetation increased, and Z0m peaked in August. In particular, the change from May to June is very significant. It may be due to the beginning of the summer monsoon in June, which led to the increase of precipitation, which accelerated the growth of vegetation and the rapid rise of Z0m. In June, July, and August, due to the continuous precipitation and rising temperature, the vegetation grows very vigorously, but it does not change after it grows to maturity. The corresponding maximum value of Z0m in the figure remains unchanged, but due to sufficient in these three months, the Z0m large value area gradually expanded, and reached the maximum range in August. From September to December, as the plateau summer monsoon retreat, the temperature and humidity are gradually reduced. Compared with the plateau summer monsoon, the vegetation is no longer suitable for vegetation growth, the contribution of vegetation to Z0m is weakened, and the surface vegetation height is the coverage gradually decreases, and thus, Z0m continues to decrease, and the range of large-value regions also gradually decreases.

**Figure 3 about here**

**Figure 4 about here**

Figures 4 and 5 respectively show the retrieved monthly surface roughness in the BJ area in

2010 and 2012. It can also be seen that the Z0m also showed a decrease from January to February in the Nagqu area in 2010 and 2012. Since February, Z0m has started to increase. Since June, Z0m has grown rapidly and reached the peak of the whole year in August. After that, Z0m began to decrease.

**Figure 5 about here**

It can also be seen from Fig. 3, Fig. 4, Fig. 5 that Z0m changes with spatial and temporal scale. Z0m shows different trends on different underlying surfaces. It is worth noting that in November 2008, the Z0m in the Nagqu area was small overall, generally as low as 1 cm. According to historical data, it is known that there is a large-scale snowfall process in the Nagqu area at this time. The snowfall of the meadow causes the underlying surface of the meadow to be homogeneous and flat, and after the snowfall falls, it is easy to form a block, scattered and discontinuous underlying surface. And it can be obtained later that the surface roughness of the area with ice and snow as the underlying surface is not more than 1 cm, which is consistent with the historical weather process. So, we think that snowfall caused the Z0m in November to be very small. And from November to December, Z0m showed a growing trend, which may be due to temperature, soil unfrozen or other reasons, resulting in the melting of snow, and then the surface roughness showed a growing trend (Zhou, 2017).

### 3.3 Evaluation of satellite data retrieved results

**Figure 6 about here**

The underlying surfaces of the three sites selected in this study are all alpine meadows. In Figure 6, the NPAM site data calculation results are larger than the satellite data retrieved results throughout the year, only September and October are very close, and the trend is similar. The maximum value of the site data calculation is 5cm and the satellite data retrieved result is 4.5cm maximum. The maximum difference is in May, which is 1.7cm. The NAMCO station data calculation results are very close to the satellite data retrieved results from April to November, but the satellite data retrieved results in January, March and December are significantly larger than the site data calculation results. The biggest difference appears in January, and the difference value is up to 1.5cm. In 2008, the calculation results of BJ station data were larger than the satellite data retrieved results throughout the year. The calculation results of the site data were very close to the satellite data retrieved results from January to April, July to November, but there was a big

298 difference between the May June and December, and the biggest difference occurred in May, with
299 a difference of 1.8 cm. In 2012, BJ's site data calculation results were consistent with the satellite
300 data retrieved results for the whole year, but the site data calculation results were larger than the
301 satellite data retrieved results from March to June, and the station data calculation results were
302 smaller than the satellite data retrieved at other times. As a result, the largest difference occurred
303 in June with a difference of 1.1 cm. It can be seen from Figure 6 that, in the overall situation, in
304 January, February, March, November and December, the seasonal variation trend of the site data
305 calculation results is consistent with the satellite data retrieved results. However, the site data
306 calculation results from April to October are greater than the satellite data retrieved results. From
307 Fig. 6 the Z0m calculated from the site observation data is larger than the satellite data, which may
308 be because the average smoothing effect. It is worth noting that from February to July, the single
309 point Z0m value was significantly increased according to the independent method of determining
310 the surface roughness, while the results obtained by using the satellite data did not increase
311 significantly. The satellite results show that the January to May, November, and December are
312 basically stable below 2cm, and only change from June to October; this is related to the
313 overlapping averages effect of satellite data retrieved. In general, the results calculated by the
314 station are generally larger than those obtained by satellite retrieved.
315 Figure 7 about here
316 The Z0m scatter plot is shown in Figure 7. It can be seen that there is a significant positive
317 correlation between retrieved by using the satellite and the surface roughness calculated from the
318 site data. The correlation coefficient between the observation result and the retrieved result except
319 for the NAMCO station in 2010 in Fig. 7(g) are large. It shows that the average result of the
320 underlying surface smoothed the same underlying surface results in different regions, further
321 indicating that the satellite retrieved results are well with the site calculation results. However, the
322 results of the NAMCO site are different from those of other sites. The correlation coefficient with
323 the average results of the underlying surface is 0.83, and the correlation coefficient with the
324 satellite retrieved results is 0.62. Or because the Namco Observation Station is closer to the lake
325 (1km), it is more affected by local microclimate such as lake and land winds. The results in Figure

7 all passed the F test of P = 0.05. It indicates that there is no significant difference between the site data calculation results and the satellite data retrieved results.

# 4 Variation characteristics of surface roughness of different underlying surfaces

According to the vegetation data GLC2009 combined with local actual conditions, the 200×200km$^2$ area of Nagqu was divided into 10 different underlying surfaces (Arino et al., 2010), namely: mountain grassland, shrub meadow, mountain meadow, alpine Grasslands, alpine meadows, sparse vegetation lap, urban land, bare land, water bodies, ice sheets and snow covers.

**Figure 8 about here**

The monthly variation of Z0m in different underlying surfaces in Nagqu area is shown in Fig. 8. It shows that 14 different underlying surfaces in the Nagqu area can be divided into four categories. The first category is urban land, accounting for 0.07% of the whole study area. The Z0m of this type of underlying surface is greater than that of other types throughout the year, and the change of Z0m is very large, probably due to the irregular changes in the underground areas of the selected areas and the irregularities caused by human activities. The second category is lush grassland, including shrub meadows, mountain grasslands, alpine grasslands and mountain meadows, which account for 62.49% of the area. The variation curves of Z0m of the four underlying surfaces are similar, and Z0m of the urban land is only smaller than that of other underlying surfaces. The third category is sparse grassland, including alpine sparse vegetation, alpine meadows and bare land, accounting for 33.74% of the area. The Z0m of the three underlying surfaces are similar, at a medium height. The Z0m of the bare soil is at the lowest point of these underlying surface Z0m, and the Z0m of the alpine meadow is relatively stable and less affected by the outside. The fourth category is ice and snow, including ice sheets and snow cover, water bodies two kinds of underlying surfaces, accounting for 3.7% of the area. The Z0m of these three underlying surfaces presents another phenomenon. The variation range of the whole year is relatively small, and the Z0m of these underlying surfaces is also small. It is more than 1cm in mid-June, and other times Z0m is less than 1cm. Figure 8(d) shows the multi-year average seasonal variation of Z0m. It can be clearly seen from the figure that the underlying surface can be

355 divided into four categories due to the difference in surface roughness. And the change from
356 January to May Z0m is very small, peaking from May to August, and then down to the previous
357 January to May level in November and December. Due to the snowfall in November 2008, it may
358 lead to the low level of November in Figure 8(d). In fact, the surface roughness on November
359 should be higher than that on December in former years.

360 It can also be seen from Fig. 8 that in the Nagqu area, except for the area of the fourth type of
361 underlying surface, the Z0m change in other areas decreases from January to February, and begins
362 to increase after February, reaching the peak on August, then starting to decrease. However, it can
363 be clearly seen from Fig. 6 that there are several stages in which Z0m changes significantly, in
364 early April, mid-May, early July, late August, and late September. The change at the end of August
365 was the most obvious. Each of the underlying surfaces Z0m changes by more than 2 cm on
366 average. The extent of the change in late September was also large, with an average change of
367 more than 1.5 cm. It should also be pointed out that the change in early July was special because
368 the change resulted in a significant increase in the Z0m of water bodies and ice.

369 It is worth noting that due to factors such as cloud cover, May, August, and November of
370 2008; August and September of 2010; April and July of 2012, the overall Z0m has changed
371 significantly. This resulted in two very significant changes in August and November on the
372 three-year average. In November, according to other meteorological data, it was caused by
373 snowfall. The reason for the August change caused by 2008 and 2010, through analyzing to the
374 Z0m of the water body and the ice and snow surface suddenly increased, was caused by
375 precipitation. Combined with several changes in Z0m, it can be analyzed that precipitation,
376 snowfall, and snow accumulation will make the underlying surface more uniform and flat, and the
377 Z0m will also be relatively reduced.

## 378 5 Conclusion and discussion

379 Through the calculation and analysis of the surface roughness of the Nagqu area in the
380 central of the Tibetan Plateau, and comparing the retrieved of the satellite data with the calculation
381 results of the observational data, the attained main conclusions are as follows:

382 (1) The retrieved results of the satellite data are basically consistent with the calculated

results of the measured data. Both indicate that the surface roughness has continued to increase from February to August, and began to decrease after reaching the peak in August, and reached the lowest value in February of the following year. There is a lot of connection between the monthly variation of surface roughness and the changes of meteorological elements brought by the plateau summer monsoon. Among them, the satellite surface retrieved results in a slow increase in surface roughness from February to May.

(2) Through the characteristics of surface roughness variation retrieved by satellite data, the underlying surface can be divided into four categories according to the surface roughness, from large to small, urban, lush grassland, sparse grassland and ice and snow. Among them, lush grassland accounts for 62.49%, $Z_{0m}$ can reach 6cm, sparse grassland accounts for 33.74%, $Z_{0m}$ can reach up to 4cm, ice and snow account for 3.7%, and $Z_{0m}$ does not exceed 1cm.

(3) Comparing the results of satellite retrieved calculation, satellite retrieved results and measured data, the results are positively correlated, and the satellite retrieved results is better fitting with the measured results. Due to the average sliding effect of the retrieved, the satellite retrieved data is smaller than the measured results. This method can be used to calculate the surface roughness results for a region and provide a true value for the model for simulation.

Through the study of surface roughness, it is beneficial to obtain the surface feature parameter values on the region, provide the ground truth value for the model input, improve the simulation level of the model in the Tibetan Plateau, and deepen the understanding of the land-atmosphere interaction process. Research on model simulation of surface flux has achieved good results in many regions (Smirnova et al., 2016). Especially in recent years, with the continuous development and improvement of numerical models, research on the applicability of different parameterization schemes in different models to different regions has continued. Luo et al. used the land surface model CoLM to conduct a single-point numerical simulation of the BJ station and successfully simulated the energy exchange process in the Nagqu area (Luo et al., 2009). Zhang et al. evaluated the surface physical process parameterization schemes of Noah LSM and Noah-MP in the entire East Asia region, and also evaluated the simulation of the surface heat flux of the Tibetan Plateau (Zhang et al., 2017). Xie et al. explored the simulation effect of land

surface model CLM4.5 in the alpine meadow area of the Qinghai-Tibet Plateau (Xie et al., 2017). Xu et al. studied the applicability of different parameterization schemes in the WRF model when simulating boundary layer characteristics in the Nagqu area (Xu, et al., 2018). Zhang, et al. Comparative analysis of the meteorological elements simulated by different land surface process schemes in the WRF model in the Yellow River source region (Zhang et al., 2019). However, the applicability of the model in the Tibetan Plateau needs further study. The terrain of the Tibetan Plateau is complex, the underlying surface is very uneven, and has high spatial heterogeneity. Because the condition of the underlying surface has a very significant impact on the surface flux, obtaining information on the surface vegetation status of a certain area is very helpful for analyzing the spatial representation of the surface flux. This study uses remote sensing images and aerodynamic roughness remote sensing retrieved model to estimate the spatial scale of aerodynamic roughness conditions in northern Tibet, which will provide parameters and parameterization scheme improvements for model simulations to study the spatial distribution of surface flux in the Tibetan Plateau.

**Acknowledgements:**

This work was financially supported by the Second Tibetan Plateau Scientific Expedition and Research (STEP) program (Grant No. 2019QZKK0103), the National Natural Science Foundation of China (Grant No. 41675106) and National key research and development program of China (2017YFC1505702)

# References:

Arino O, Ramos J, Kalogirou V, et al.“Glob Cover 2009”[R].Edinburgh, UK：Proceedings of the living planet Symposium, 2010.

Asrar , G ., Myneni , R.B.and Chaudhury , B.J., 1992, Spatial heterogeneity in vegetation canopies and remote sensing of observed photosynthetically active radiation:a modeling study , Ren.Sens.Env ., 41, 85～103.

Brutsaert , W.A ., 1982, Evaporation into the Atmosphere , Dordrecht in Holland , D .Reidel Publishing Company,113 ～ 121.

Chu D., Basabta S., Wang W., et al, 2010. Land Cover Mapping in the Tibet Plateau Using

MODIS Imagery[J]. Resources Science, 32(11): 2152-2159. (in Chinese with English abstract)

Chen, J., Wang, J., Mitsuaki, H., 1993. An independent method to determine the surface roughness length. Chin. J. Atmos. Sci. 1993, 17, 21–26. (in Chinese with English abstract)

Chen Q., L. Jia, R. Hutjes, M. Menenti, 2015, Estimation of Aerodynamic Roughness Length over Oasis in the Heihe River Basin by Utilizing Remote Sensing and Ground Data, Remote Sensing, 2015, 7(4), 3690-3709; doi:10.3390/rs70403690.

Chen X., et al, 2013. An improvement of roughness height parameterization of the Surface Energy Balance System (SEBS) over the Tibetan Plateau[J]. Journal of Applied Meteorology and Climatology, 52(3): 607-622.

Guan X., Huang J., et al, 2009. Variability of soil moisture and its relationship with surface albedo and soil thermal parameters over the Loess Plateau[J]. Advances in Atmospheric Sciences, 26(4): 692-700, doi: 10.1007/s00376-009-8198-0.

Högström U., 1996 'Review of Some Characteristics of the Atmospheric Surface Layer' Boundary-Layer Meteorol 78 215–246 10.1007/BF00120937

Irannejad P, Shao Y P, 1998. Description and validation of the atmosphere-land-surface interaction scheme(ALSIS)with HAPEX and Cabauw data[J]. Global Planet Change, 19(1): 87-114.

Jane Q., 2008. The third pole[J]. Nature, 454(24): 393-396.

Jia L., Wang J., Hu Z., 2000. The Characteristics of Roughness Length for Heat and Its Influence on Determination of Sensible Heat Flux in Arid Zone[J]. Plateau Meteorology, 19(04): 495-503. (in Chinese with English abstract)

Li F., Li S., Chen T., 2004. A Study on Develpoment of the Tibetan North Grasslands Tourism Stockbreeding in Naqv Tibet[J]. Sichuan Caoyuan, 109(12): 38-42. (in Chinese with English abstract)

Li J., Hong Z., Sun S., 2000. An Observational Experiment on the Atmospheric Boundary Layer in Gerze Area of the Tibetan Plateau[J]. Chinese Journal of Atmospheric Sciences, 24(03): 301-312. (in Chinese with English abstract)

Li L., Chen X., Wang Z., et al, 2010. Climate Change and Its Regional Differences over the Tibetan Plateau[J]. Advances in Climate Change Research, 6(03): 181-186. (in Chinese with

English abstract)

Liu J., Zhou M., Hu Y., 2007. Discussion on the Terrain Aerodynamic Roughness[J]. Ecology and Environment, 16(06): 1829-1836. (in Chinese with English abstract)

Luo S., Lü S., Yu Z. (2009) Development and validation of the frozen soil parameterization scheme in Common Land Model. Cold Reg Sci Technol 55:130–140

Ma Y., Tsukamoto O, Wang J., et al, 2002. Analysis of aerodynamic and thermodynamic parameters on the grassy marshland surface of Tibetan Plateau[J]. Progress in Natural Science, 12(1): 36-40.

Ma Y., Wang J., et al, 2002. Analysis of Aerodynamic and Thermodynamic Parameters on the Grassy Marshland Surface of Tibetan Plateau[J]. Peogress in Natural Science, 12(01): 36-40. (in Chinese with English abstract)

Ma Y., Yao T., Wang J., et al, 2006. The Study on the Land Surface Heat Fluxes over Heterogeneous Landscape of the Tibetan Plateau[J]. Advances in Earth Science, 21(12): 1215-1223. (in Chinese with English abstract)

Massman W., 1997. An analytical one-dimensional model of momentum transfer by vegetation of arbitrary structure[J]. Boundary-Layer Meteorology, 83(3): 407-421.

Massman W., 1999. An analytical one-dimensional second-order closure model of turbulence statistics and the Lagrangian time scale within and above plant canopies of arbitrary structure[J]. Boundary-Layer Meteorology, 91(1): 81-107.

Monin A., Obukhov A., 1954. Basic laws of turbulent mixing in the atmosphere near the ground[J]. Tr Akad Nauk SSSR Geofiz Inst, 24(15): 163-187.

Moran, M .S ., Clarke , T .H., Inone, Y.et al., 1994, Estimating crop water deficit using the relation between surface-air temperature and spectral vegetation index, Rem .Sens. of Env ., 49 , 246 ～ 263.

Panosky H., Dutton J., 1984. Atmospheric Turbulence: Models and Methods for Engineering Applications[M]. New York: John Wiley, 1-399.

Pierce , L.L., Walker, J., Downling , T .I.et al., 1992, Ecological change in the Murry -Darling Basin-III :A simulation of regional hydrological changes , Journal of Applied Ecology , 30, 283～

294.

Raupach, M .R., 1994, Simplified expressions for vegetation roughness leng h and zero-plane displacement as functions of canopy height and area index , Boundary -Layer Meteor ., 71, 211-216.

Shao Y., 2000. Phtsics and Modeling of Wind Erosion[M]. London: Kluwer Academic Publishers, 1-452.

Smirnova T., Brown J., Benjamin S., Kenyon J. (2016) Modifications to the rapid update cycle land surface model (RUC LSM) available in the weather research and forecasting (WRF) model. Mon Weather Rev 144(5):1851–1865

Stanhill G., 1969. A simple instrument for the field measurement of turbulent diffusion flux. J Appl Meteorol 8:509–513

Stull B R, 1991. An Introduction to Boundary Layer Meteorology[M]. Beijing: China Meteorological Press, 1-737.

Su B., Zhao M., Ren J., 1999. Influence of Scalar Roughness Lengths on the Biosphere-Atmosphere Transfer[J]. Chinese Journal of Atmospheric Sciences, 23(03): 349-358. (in Chinese with English abstract)

Su, Z., 1996. Remote Sensing Applied to Hydrology: The Sauer River Basin Study. RuhrUniversität Bochum, Lehrstuhl für Hydrologie, Wasserwirtschaft und Umwelttechnik.

Tao S., Chen, L., Xu X., et al, 1998. Progresses of the Theoretical Study in the Second Tibetan Plateau Experiment of Atmospheric Sciences (PartI)[M]. Beijing: China Meteorological Press, 1-348.

Wang J., 1999. Land Surface Process Experiments and Interaction Study in China-from HEIFE to Imgrass and GAME-TIBET/TIPEX[J]. Plateau Meteorology, 18(03): 280-294. (in Chinese with English abstract)

Wu G., Mao J., Duan, A., et al., 2004. Recent progress in the study on the impact of Tibetan Plateau on Asian summer climate[J]. Acta Meteorologica Sinica, 62(5): 528-540. (in Chinese with English abstract)

Wu G., Zhang Y., 1998. Tibetan Plateau forcing and timing of the Mon-soon onset over south Asia

and the south China sea[J]. Monthly Weather Review, 4(126): 913-927.

Wu G., Zhang Y., 1999. Thermal and Mechanical Forcing of the Tibetan Plateau and Asian Monsoon Onset.Part Ⅱ:Timing of the Onset[J]. Chinese Journal of Atmospheric Sciences, 23(01): 52-62. (in Chinese with English abstract)

Wu G., Liu Y., Liu X., et al. 2005. How the heating over the Tibetan Plateau affects the Asian climate in summer[J]. Chinese Journal of Atmospheric Sciences, 29(1): 47-56. (in Chinese with English abstract)

Wu X., Ma W., Ma Y., 2013. Observation and Simulation Analyses on Characteristics of Land Surface Heat Flux in Noethern TibetanPlateau in Summer[J]. Plateau Meteorology, 32(05): 1246-1252. (in Chinese with English abstract)

Xie Z., Hu Z., Liu H., Sun G., et al., 2017 Evaluation of the Surface Energy Exchange Simulations of Land Surface Model CLM4.5 in Alpine Meadow over the Qinghai-Xizang Plateau. Plateau Meteorology, 36(1): 1-12. (in Chinese with English abstract)

Xu L., Liu H., Xu X., et al. 2018, Applicability of WRF model to the simulation of atmospheric boundary layer in Nagqu area of Tibetan Plateau[J]. Acta Meteorologica Sinica, 2018(6):955-967. (in Chinese with English abstract)

Xun X., Hu Z., Ma Y., 2012. The dynamic Plateau Mon-soon Index and its association with general circulation an omaliesming[J]. Advances in Atmospheric Sciences, 29(6): 1249-1263, DOI: 10.1007/s00376-012-1125-9.

Yang M., Yao T., 1998. A Review of the Study on the Impact of Snow Cover in the Tibetan Plateau on Asian Monsoon[J]. Journal of Glaciology and Geocrylolgy, 20(2): 90-95. (in Chinese with English abstract)

Ye D., Wu G., 1998. The role of heat source of the Tibetan Plateau in the general circulation[J]. Meteorological and Atmospheric Physics, 67(1): 181-198.

Zhang G., Zhou G., Chen F. 2017, Analysis of Parameter Sensitivity on Surface Heat Exchange in the Noah Land Surface Model at a Temperate Desert Steppe Site in China[J]. Acta Meteorologica Sinica. (6).1167-1182.doi:10.1007/s13351-017-7050-1.

Zhang Q., Lv S., 2003. The Determination of Roughness Length over City Surface[J]. Plateau

Meteorology, 22(01): 24-32. (in Chinese with English abstract)

Zhang Y., Wu G., 1998. Diasnostic Investigations of Mechanism of Onset of Asian Summer Monsoon and Abrupt Seasonal Transitions Over Northern Hemisphere PartI[J]. Acta Meteorologica Sinica, 56(5): 2-17. (in Chinese with English abstract)

Zhou X., Zhao P., Chen J., et al, 2009. Impacts of Thermodynamic Processes over the Tibetan Plateau on the Northern Hemispheric Climate[J]. Sci China Ser D-Earth Sci, 39(11): 1473-1486. (in Chinese with English abstract)

Zhou, Y., Ju, W., Sun, X., Wen, X., Guan, D. 2012 Significant decrease of uncertainties in sensible heat flux simulation using temporally variable aerodynamic roughness in two typical forest ecosystems of China. J. Appl. Meteorol. Climatol. 2012, 51, 1099–1110.

Zhou Y., Xu W., Bai A., et al, 2017. Dynamic Snow-melting Process and its Relationship with Air Temperature in Tuotuohe, TibetanPlateau[J]. Plateau Meteorology, 36(1): 24-32. (in Chinese with English abstract)

565 Figure captions

566 Fig. 1 The location of sites and the land cover on the northern of the Tibetan Plateau. The black

567 solid circle '●' is location of the sites

568 Fig. 2 The surface roughness length of different site on the northern of the Tibetan Plateau

569 Fig. 3 The surface roughness length on the northern of the Tibetan Plateau in 2008

570 Fig. 4 The surface roughness length on the northern of the Tibetan Plateau in 2010

571 Fig. 5 The surface roughness length on the northern of the Tibetan Plateau in 2012

572 Fig. 6 Comparison of surface roughness length by site observation and satellite remote sense

573 retrieved

574 Fig. 7 Scatter plots of the retrieved and calculated surface roughness length at four sites

575 Fig. 8 The curve of the surface roughness length in different underlying surface

576

577 Tables

578 Table. 1 The legend of the land cover map on the northern of the Tibetan Plateau

| Value | Color | Land Cover Types | Percent（%） |
|---|---|---|---|
| 11 | | Mountain grassland | 5.79 |
| 14 | | Shrub meadow | 3.25 |
| 20 | | Mountain meadow | 8.26 |
| 30 | | Alpine grassland | 45.16 |
| 70 | | Needleleaved evergreen forest | 0.23 |
| 100 | | Mixed forest | 0.03 |
| 110 | | Mixed forestland and grassland | 0.06 |

579

| Value | Color | Land Cover Types | Percent （%） |
|---|---|---|---|
| 120 | | Mixed grassland and | 0.04 |
| 140 | | Alpine meadow | 28.28 |
| 150 | | Alpine sparse vegetation | 0.29 |
| 190 | | Urban areas | 0.07 |
| 200 | | Bare areas | 4.90 |
| 210 | | Water bodies | 2.57 |
| 220 | | Permanent Snow and ice | 1.07 |

580

581

582

583

584

585

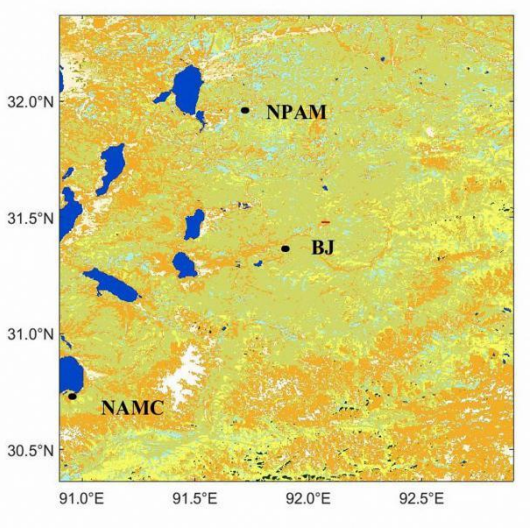


586

587 Fig. 1 The location of sites and the land cover on the northern of the Tibetan Plateau. The black

588 solid circle '●' is location of the sites.

589

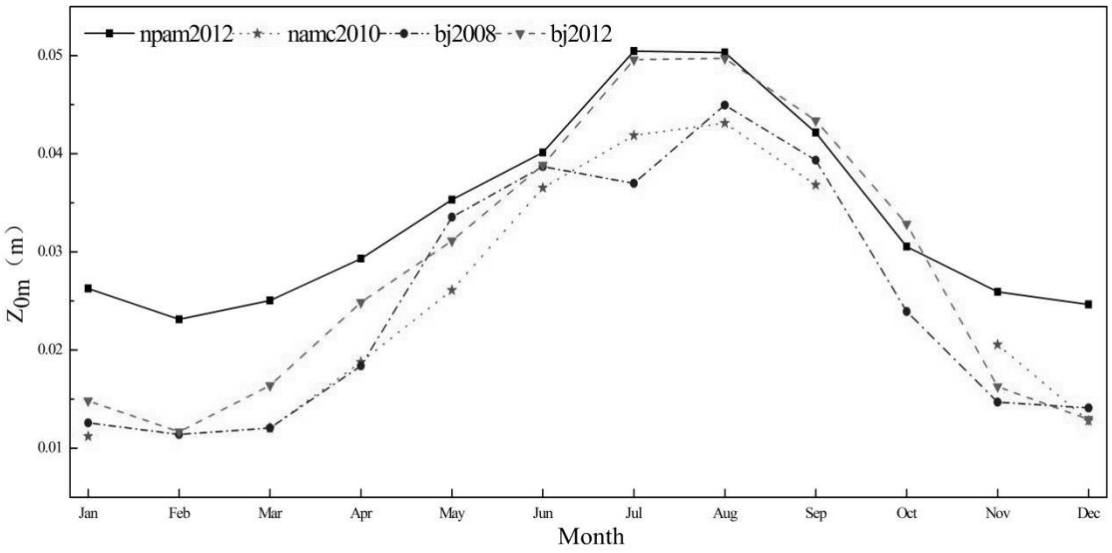


590

591 Fig. 2 The surface roughness length of different site on the northern of the Tibetan Plateau

592

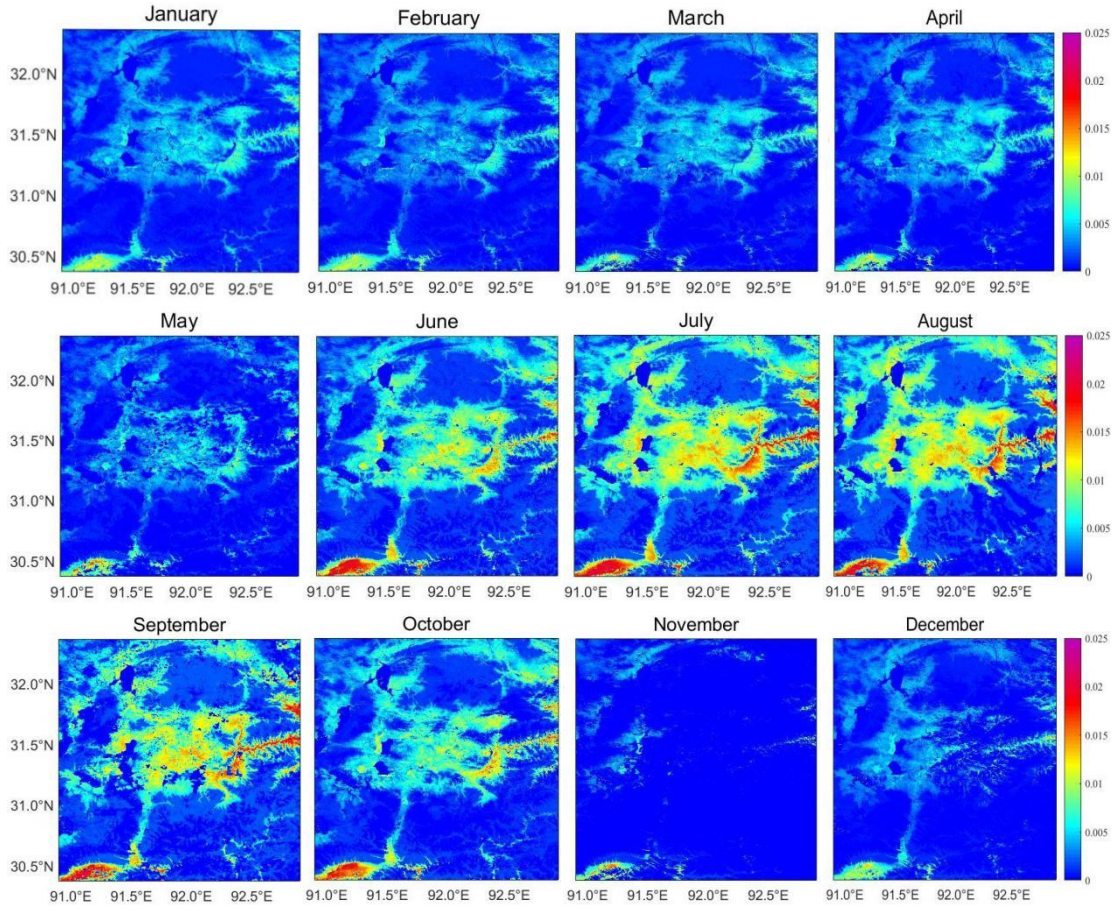


Fig. 3 The surface roughness length on the northern of the Tibetan Plateau in 2008

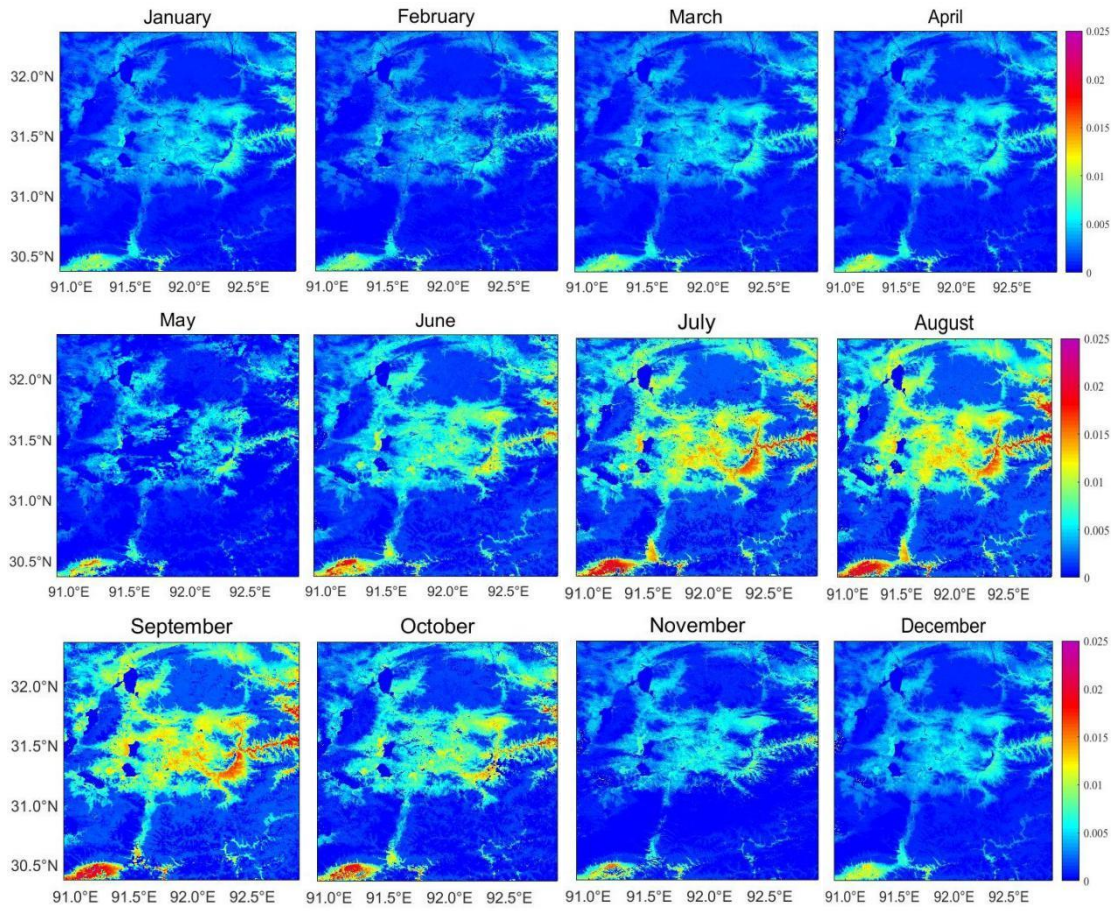


Fig. 4 The surface roughness length on the northern of the Tibetan Plateau in 2010

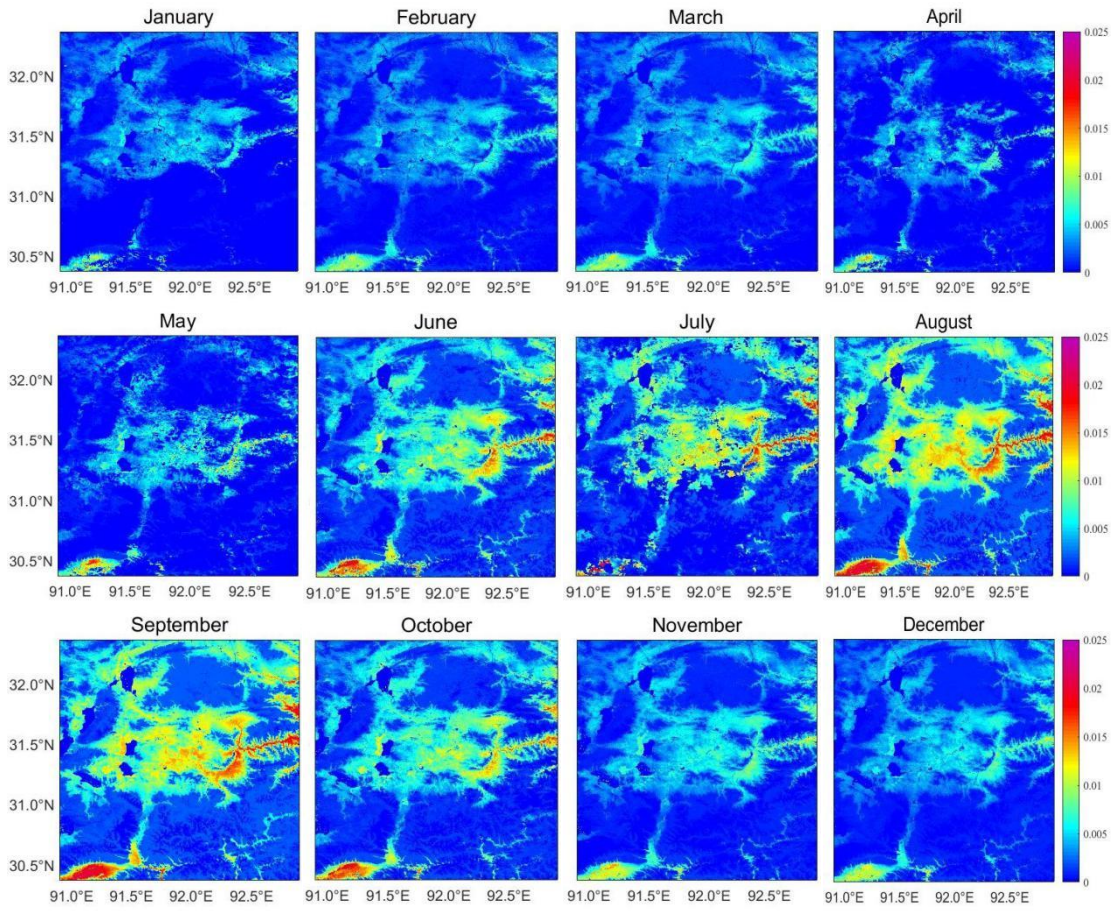


Fig. 5 The surface roughness length on the northern of the Tibetan Plateau in 2012

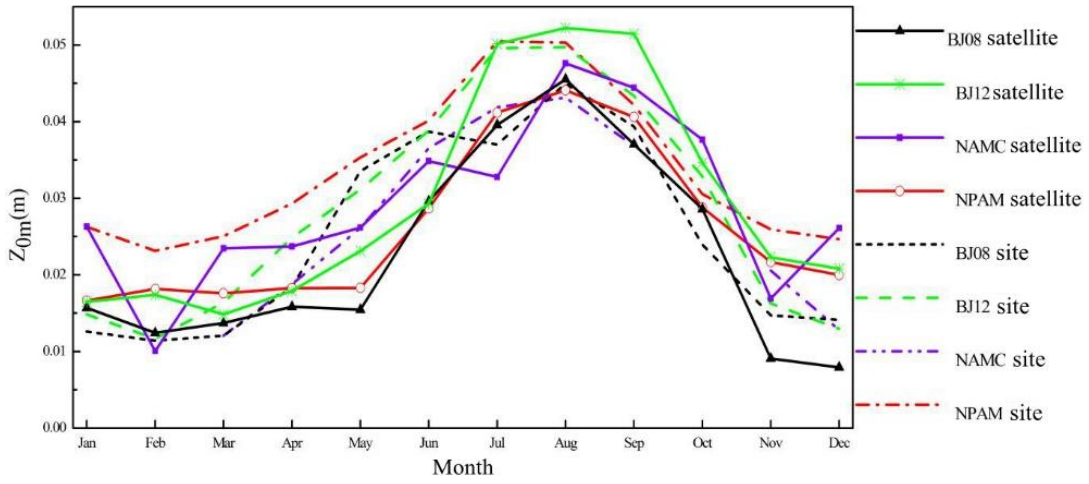


610

611 Fig. 6 Comparison of surface roughness length by site observation and satellite remote sense

612 retrieved

613

614

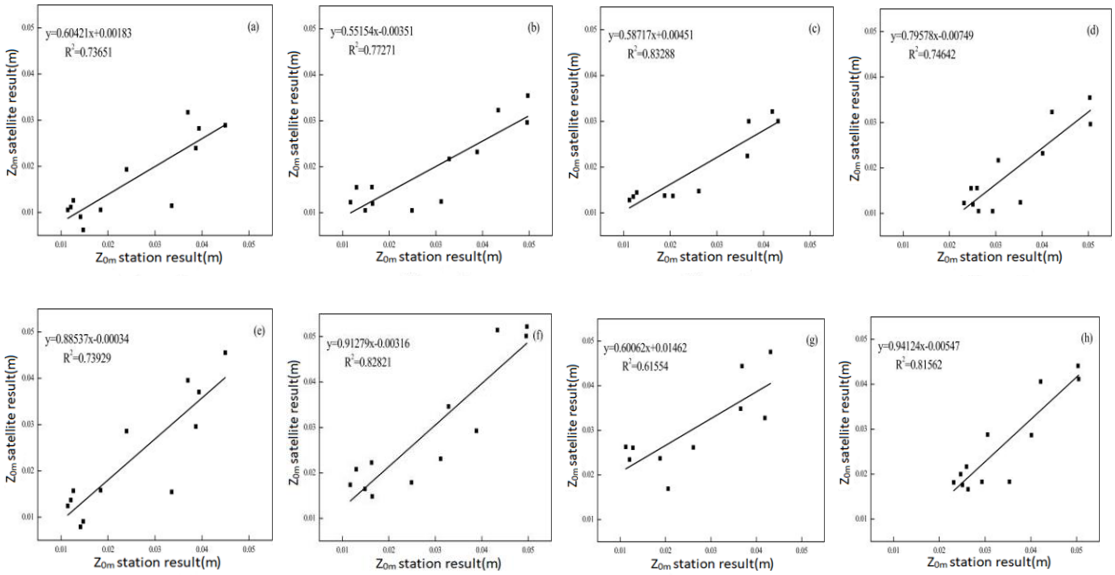


615

616 Fig. 7 Scatter plots of the retrieved and calculated surface roughness length at four sites

617 (a-d: scatter plot of the observation results and the average result of the underlying surface; e-h：

618 scatter plot of the observation and retrieved results; a,e: BJ station in 2008; b,f: BJ station in 2012;

619 c,g: NAMC station in 2010; d,h: NPAM station in 2012)

620

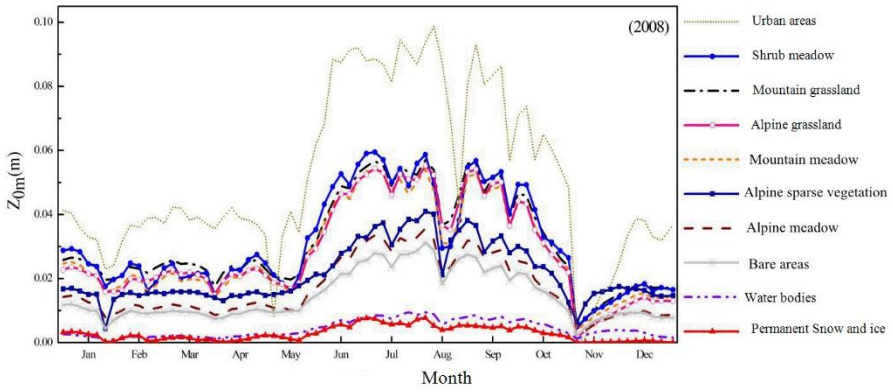


621

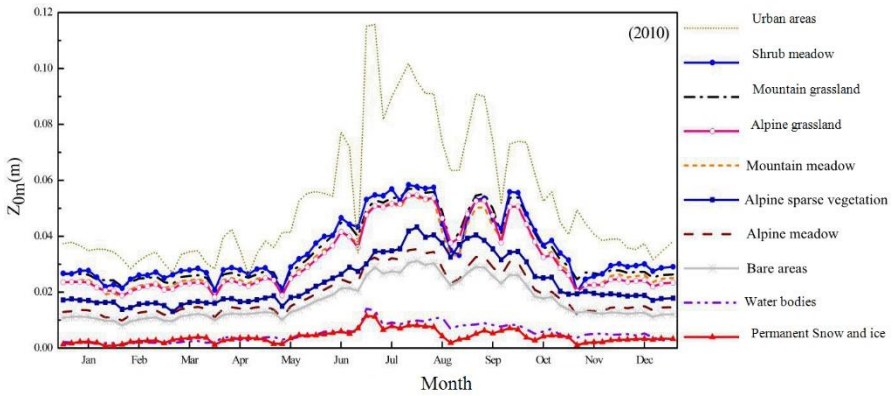


622

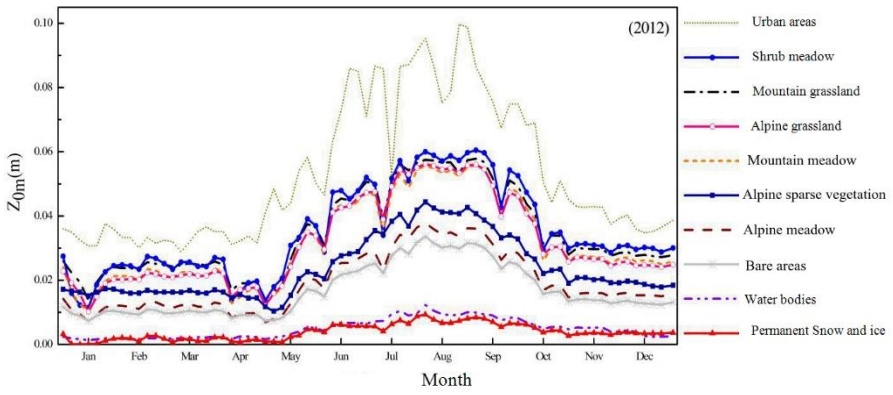


623

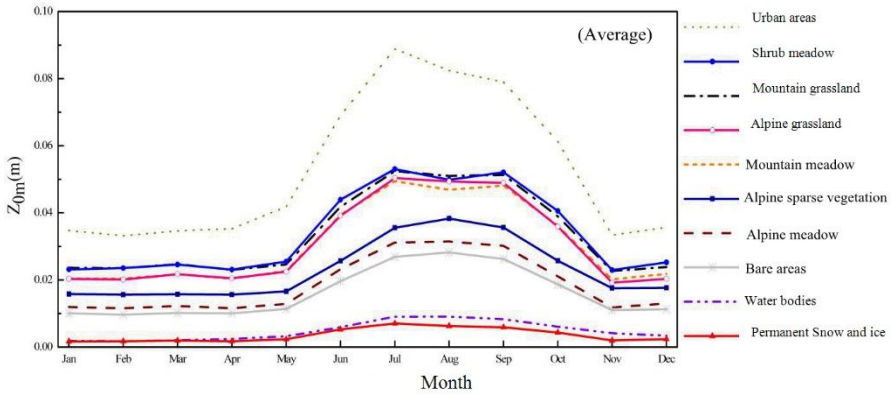


624

625 Fig. 8 The curve of the surface roughness length in different underlying surface

626